NANO LETTERS

2005
Vol. 5, No. 3
507−510

Photocurrent Imaging of Charge Transport Barriers in Carbon Nanotube Devices

Kannan Balasubramanian,[†] Marko Burghard,*[,†] Klaus Kern,[†] Matteo Scolari,[‡] and Alf Mews[‡]

Max-Planck-Institut für Festkoerperforschung, Heisenbergstrasse 1, D-70569 Stuttgart, Germany, and Institut für Physikalische Chemie, Universität Mainz, D-55099 Mainz, Germany

Received January 11, 2005

ABSTRACT

The realization of high-performance electrical devices incorporating single-wall carbon nanotubes critically depends on the minimization of charge transport barriers in the tubes and at the contacts. Herein we demonstrate photocurrent imaging as a fast and effective tool to locate such barriers within individual metallic nanotubes contacted by metal electrodes. The locally induced photocurrents directly reflect the existence of built-in electric fields associated with the presence of depletion layers at the contacts or structural defects along the tubes.

Single-wall carbon nanotubes (SWCNTs) represent attractive building blocks for ultrasmall electronic devices, for instance as nanoscale interconnects of high current carrying capability.[1] However, the successful fabrication of such devices still requires a deeper understanding of the local electronic properties of SWCNTs and their connection to leads. In this context an increasing number of studies is being directed toward the effect of structural defects and electrode contacts on the charge transport through SWCNTs both from a theoretical[2,3] and an experimental[4−6] point of view. To obtain molecular-scale information on the electronic structure along electrically contacted SWCNTs, various scanning probe techniques have been applied. These include scanning gate microscopy (SGM),[5,6] conducting tip atomic force microscopy (CT-AFM),[7] as well as electrostatic AFM (EFM).[4,8] However, while these methods offer a good lateral resolution, they do not allow for rapid scanning over extended surface regions, which would be highly desirable in order to assess the structural and electronic perfection of larger tube ensembles in an economic time scale. Here, we demonstrate that photocurrent mapping[9] fulfills this requirement and constitutes a powerful tool to probe local variations in the electronic structure along individual, electrically addressable nanotubes. Furthermore, as the locally induced photocurrent response is sensitive to the presence of built-in electric fields that effect the separation of generated electrons and holes, it allows to directly reveal energy barriers inside nanotubes or at their interface to the metal contacts—information that until now could be obtained only indirectly from electrical transport studies.[10−12]

The experimental setup in the present study consists of a confocal optical microscope wherein the electrical transport properties of individual SWCNTs can be measured in situ under illumination with circularly polarized light that is focused through a high numerical aperture (NA) objective (10×; NA 0.25 or 50×; NA 0.6).[9,13] The samples were fabricated by depositing SWCNTs obtained from the arc discharge (Carbolex) or HiPCO process on a degenerately doped Si substrate with a thermally grown SiO_2 layer of 100 or 200 nm thickness. Subsequently, 10 μm wide electrodes with a spacing of ∼1.3 μm were defined by e-beam lithography on top of individual tubes. The electrodes were made of 15 nm AuPd with a 0.5 nm thick Ti adhesion layer. Metallic tubes were selected based on their minor gate dependence of conductance. The samples exhibited room-temperature conductances in the range of 0.5 to 38 μS at zero gate voltage.

Photoelectronic transport (PET) images were acquired by recording the drain current (I_{ds}) at zero drain-source bias (V_{ds}). For this purpose, the contacted sample is illuminated by scanning through the focus of the optical microscope (excitation wavelength $\lambda_{exc} = 514.5$ nm with a power of 1 mW) and the local photocurrent is plotted using a false color scale. Our experiments performed on a total of 12 metallic SWCNTs revealed two different categories of PET images. While the first type of samples (type I) exhibited

* Corresponding author. Tel: +49.711.6891448, Fax: +49.711.6891662, E-mail: m.burghard@fkf.mpg.de.
[†] Max-Planck-Institut für Festkoerperforschung.
[‡] Universität Mainz.

10.1021/nl050053k CCC: $30.25
Published on Web 02/18/2005

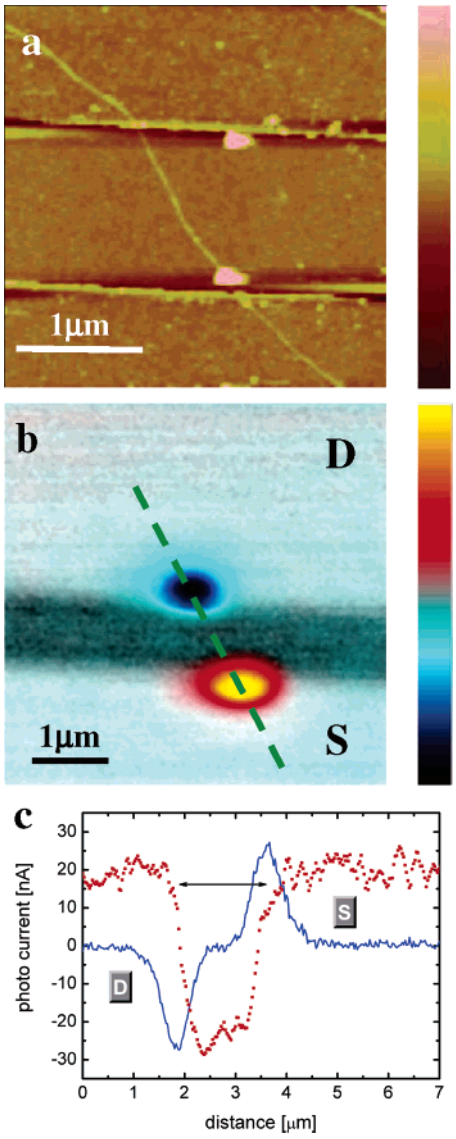

Figure 1. Photoelectronic transport (PET) imaging of an individual metallic SWCNT. (a) Atomic force microscope (AFM) topograph of the sample showing the two electrodes contacting a single metallic SWCNT of diameter 1.3 nm. (b) PET image of the same sample obtained by recording the drain current at zero bias, overlayed over a simultaneously taken reflection image. (S − source, D − drain, λ_{exc} = 514.5 nm, 50× objective, 1 mW). (c) The blue solid line and the red dotted line show respectively the line profiles of the photocurrent and the reflection signal along the green line marked in (b). The height scale is 25 nm for (a) and the current scale is ±27 nA for (b).

one spot at each of the two metal contacts, the samples of type II revealed at least one additional spot along the tube.

Figure 1a displays the AFM image of a representative sample of type I, comprising an apparently homogeneous nanotube with no discernible structural defect. At high drain−source bias (V_{ds}), the dark current through the tube was found to saturate at 25 μA, in accordance with previous observations on individual metallic SWCNTs.[14] Figure 1b displays the PET image obtained at zero-bias for this sample. Two oppositely signed lobes can be clearly identified in the PET image close to the contacts, as can also be inferred from the line profiles of the reflection and PET images shown in

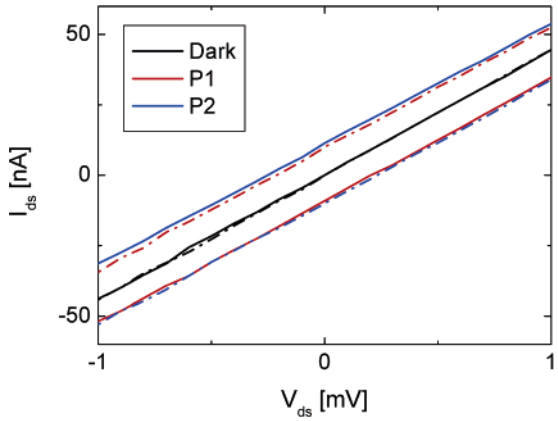

Figure 2. Low-bias I_{ds} versus V_{ds} curves obtained without illumination (black lines), with the laser spot positioned at the top lobe (P1, red lines), and with the laser spot at the bottom lobe (P2, blue line) of the PET image shown in Figure 1. The solid lines are obtained with the top electrode being drain and the bottom electrode being source. The broken lines are obtained upon exchanging source and drain. The creation of an offset photovoltage at the contacts can be inferred from these measurements. (λ_{exc} = 647.1 nm, 10× objective, 1 mW).

Figure 1c. Similar results were obtained on this sample with another laser wavelength (λ_{exc} = 647.1 nm, 1 mW) or by using a lower magnification objective (10×), although in both cases the photocurrents were smaller and the sizes of the lobes larger. Figure 2 displays the low-bias $I-V$ curves measured while shining laser light at the positions of the two lobes. It is evident from here that the generated short-circuit current manifests itself as an offset voltage. Accounting for the resistance of the tube, the associated offset photovoltage is calculated to be ≈0.2 mV, as extracted from the shift of the linear curves. The sign of this offset is found to be opposite for the two lobes, in accordance with the results displayed in Figure 1.

We interpret the substantial photocurrents generated at the metal contacts to result from local energy barriers introduced when the tube comes in contact with the metal electrode. The nanotube in Figure 1 has a conductance of ∼e^2/h at room temperature, considerably lower than the value of $4e^2/h$ expected for ballistic transport through an ideally contacted metallic tube with two conductance channels.[15] This difference can be ascribed to the combined effect of scattering by acoustic phonons[16] and reflections by potential barriers at the tube/metal contacts.[10] The importance of the latter is apparent from the fact that the resistance of the tube increased upon cooling the tube to 2 K, with the sample exhibiting a suppression of conductance near V_{ds} = 0 and a temperature-dependent zero-bias anomaly.[12] In principle, the reduction in conductance from the ideal value could also be partially due to defects along the nanotube. However, a substantial gate dependence of conductance would then be expected,[5] which was not observed for this sample. This leads us to conclude that for the present nanotube, the barriers at the contacts restrict the charge transport. Although metallic SWCNTs with nearly perfect contacts have been demonstrated using pure palladium,[17] nanotubes contacted with other metals, such as in the present case, generally exhibit

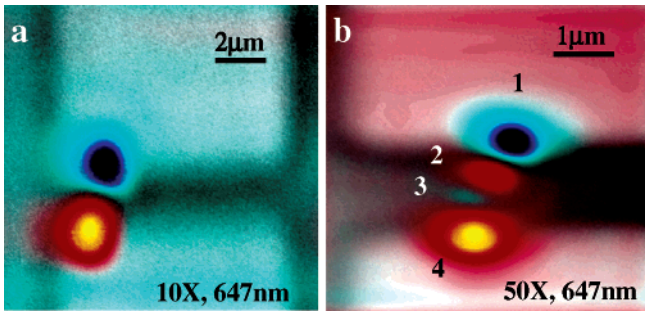

Figure 3. PET images obtained with a defective contacted metallic nanotube using (a) a 10× objective at 647.1 nm and (b) a 50× objective at 647.1 nm. Additional lobes in the gap between the electrodes can be identified in (b), indicative of structural inhomogeneities along the tube. Please note the different length scales of the images.

signatures of contact barriers.[10−12] This barrier formation can be ascribed to band bending as a result of charge transfer due to the equilibration of Fermi levels when the 1D nanotube and the 3D metal electrode are brought in contact.[18,19] Based on these arguments, the photovoltage generation at the metallic nanotube/AuPd interface can be understood to originate from electron/hole pairs locally created by photoexcitation, followed by the separation of electrons and holes due to the local built-in electric field. In this process, the interband transition between the first van Hove singularities in the nanotube provides the necessary absorption cross-section. This is consistent with the observation that the metallic HiPCO tubes showed larger photocurrent signals when illuminated at 514.5 nm than at 647.1 nm under otherwise identical conditions, in accordance with previous reports of stronger optical absorption for the HiPCO tubes at 514.5 nm.[20,21]

When the nanotube is brought in contact with the metal electrode, the internal electric field generated due to charge transfer is directed toward the metal electrode. Seen from the source lead, the electric field at the source contact is oriented opposite to that of the electric field at the drain contact. As a consequence, the generated photocurrents are in opposing directions at the two contacts, which explains the opposite signs of the two lobes in the PET image (Figure 1b). In all of the measured samples, the photocurrent is negative at the drain electrode (the electron flow is from source to drain), which indicates that the nanotube electronic bands experience an upward bending at the contacts, in agreement with the fact that the work function of the nanotube is smaller than that of AuPd.[19] The identical magnitude of the photocurrents generated at the two contacts of the sample in Figure 1 implies the presence of symmetric contact barriers. Some samples, however, displayed considerably different magnitudes of the peak photocurrent at the two electrodes. This finding indicates the formation of asymmetric contacts, as has been observed also on semiconducting nanotubes in other experiments.[7,9] With respect to the spatial extent of the barrier region, the fact that the lobes appear slightly elongated only in the scanning direction, but not in the direction along the tube axis, suggests a value of the order of a few nm for the depletion length, far below the resolution of the confocal microscope (≈ 250 nm).[22,23]

Representative of the samples of type II, Figure 3 compares PET images taken on another metallic tube with the 10× and 50× objectives at $\lambda_{exc} = 647.1$ nm. Whereas the 10× magnification image (Figure 3a) shows only two lobes at the edges of the electrodes, two additional lobes can be seen in the 50× magnification PET image (Figure 3b). In comparison, type I samples such as the one depicted in Figure 1 still display only the two lobes at the contacts, even under higher magnification. For the specific case of the nanotube in Figure 3, the series of lobes between the two electrodes shows a pattern of alternating signs. Analogous to the generation of two oppositely signed lobes **1** and **4** at the contacts, the observation of lobes **2** and **3** can be understood to originate from the presence of built-in electric fields in opposing directions at these locations. The AFM image of this sample (not shown here) revealed kinks at the positions of the lobes **2** and **3**. Taken together, it is reasonable to

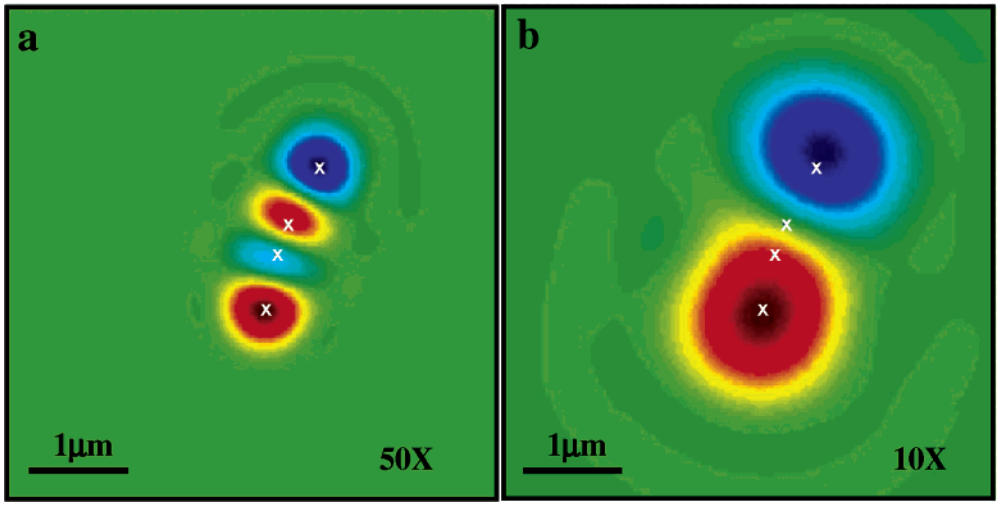

Figure 4. Simulated PET images for the sample of Figure 3, assuming point-like photoactive sites (refer text) at the center of the four lobes **1** to **4**, using 50× (a) and 10× (b) objectives. The assumed positions of the sites are overlayed over the images as four crosses. The colormap is the same as that used in Figure 1 with an arbitrary range.

assume this tube to be composed of a semiconducting segment connecting two metallic segments via defects such as pentagon−heptagon pairs.[24,25] The two metal-semiconducting junctions would behave like Schottky barriers responsible for the creation of the lobes **2** and **3**. Evidence for the existence of segments of varying chirality along individual SWCNTs has recently been gained by Raman spectroscopy.[26] The presence of such structural inhomogeneities along this tube could be further asserted due to the fact that the tube exhibited a room-temperature conductance much less than e^2/h and a sizable gate dependence of conductance.[5]

A simulation of the measured PET images could further corroborate the presence of two localized defect sites. The generation of the PET image was modeled as a linear interaction of the incident laser beam with photoactive sites along the tube. Incident beam patterns were generated separately for the 10× and 50× objectives.[27] The photoactive sites for the tube in Figure 3 were taken to be the center of the lobes **1** to **4**. The photoelectronic response is then obtained by a convolution of the beam pattern with each of these point-like photoactive sites. Varying interaction strengths were associated with these sites based on their nature as being either a contact site or a defect site. Strong photoactive sites **1** and **4** were assigned an equal magnitude of 1 with opposing signs, while comparatively weaker sites **2** and **3** were given a magnitude less than 1 in addition to having opposite signs. The result of such a simulation is shown in Figure 4. A striking similarity between the simulated and measured PET images is apparent. In particular, the extra lobes visible through the 50× objective have disappeared in the images obtained using the 10× objective. It is worth mentioning that other SWCNTs showed between one and three extra lobes, revealing a variety of patterns with respect to the sign of the photocurrent signal. Further systematic studies on the origin of these presumably defect-induced lobes are under progress.

In summary, we have demonstrated that detection of the local (photo-)electronic properties constitutes an excellent means to unravel electronic structure modulations along individual nanotubes. The sizable photocurrent signals observed at the contacts provide direct evidence for the formation of depletion regions resulting from the equilibration of the electrochemical potentials at the contact between metallic SWCNTs and metal electrodes. Moreover, the sensitivity of photocurrent mapping to structural defects makes this method highly valuable for the optimization of future optoelectronic and photovoltaic devices built from individual nanotubes.

Acknowledgment. This work was partly funded by the DFG projects BU1125/3 and ME1380/9. We are grateful to Prof. Thomas Basché and Uli Wannek for experimental support.

References

(1) Dai, H.; Wong, E. W.; Lieber, C. M. *Science* **1996**, *272*, 523.
(2) Delaney, P.; Choi, H. J.; Ihm, J.; Louie, S. G.; Cohen, M. L. *Nature* **1998**, *391*, 466.
(3) Chico, L.; Benedict, L. X.; Louie, S. G.; Cohen, M. L. *Phys. Rev. B* **1996**, *54*, 2600.
(4) Bozovic, D.; Bockrath, M.; Hafner, J. H.; Lieber, C. M.; Park, H.; Tinkham, M. *Appl. Phys. Lett.* **2001**, *78*, 3693.
(5) Bockrath, M.; Liang, W.; Bozovic, D.; Hafner, J. H.; Lieber, C. M.; Tinkham, M.; Park, H. *Science* **2001**, *291*, 283.
(6) Freitag, M.; Johnson, A. T.; Kalinin, S. V.; Bonnell, D. A. *Phys. Rev. Lett.* **2002**, *89*, 216801.
(7) Freitag, M.; Radosavljevic, M.; Clauss, W.; Johnson, A. T. *Phys. Rev. B* **2000**, *62*, R2307.
(8) Bachtold, A.; Fuhrer, M. S.; Plyasunov, S.; Forero, M.; Anderson, E. H.; Zettl, A.; McEuen, P. L. *Phys. Rev. Lett.* **2000**, *84*, 6082.
(9) Balasubramanian, K.; Fan, Y.; Burghard, M.; Kern, K.; Friedrich, M.; Wannek, U.; Mews, A. *Appl. Phys. Lett.* **2004**, *84*, 2400.
(10) Bockrath, M.; Cobden, D. H.; McEuen, P. L.; Chopra, N. G.; Zettl, A.; Thess, A.; Smalley, R. E. *Science* **1997**, *275*, 1922.
(11) Bezryadin, A.; Verschueren, A. R. M.; Tans, S. J.; Dekker, C. *Phys. Rev. Lett.* **1998**, *80*, 4036.
(12) Hunger, Th.; Lengeler, B.; Appenzeller, J. *Phys. Rev. B* **2004**, *69*, 195406.
(13) Mews, A.; Koberling, F.; Basche, T.; Philipp, G.; Duesberg, G. S.; Roth, S.; Burghard, M. *Adv. Mater.* **2000**, *12*, 1210.
(14) Yao, Z.; Kane, C. L.; Dekker, C. *Phys. Rev. Lett.* **2000**, *84*, 2941.
(15) Liang, W.; Bockrath, M.; Bozovic, D.; Hafner, J. H.; Tinkham, M.; Park, H. *Nature* **2001**, *411*, 665.
(16) Reich, S.; Thomsen, C.; Maultzsch, J. *Carbon Nanotubes: Basic Concepts and Physical Properties*, Wiley-VCH: Weinheim, 2004.
(17) Mann, D.; Javey, A.; Kong, J.; Wang, Q.; Dai, H. *Nano Lett.* **2003**, *3*, 1541.
(18) Kong, K.; Han, S.; Ihm, J. *Phy. Rev. B* **1999**, *60*, 6074.
(19) Xue, Y.; Ratner, M. A. *Phys. Rev. B* **2004**, *69*, 161402.
(20) Miyauchi, Y.; Chiashi, S.; Murakami, Y.; Hayashida, Y.; Maruyma, S. *Chem. Phys. Lett.* **2004**, *387*, 198.
(21) Zheng, N.; Bu, X.; Wang, B.; Feng, P. *Science* **2002**, *298*, 2366.
(22) Freitag, M.; Radosavljeic, M.; Yhou, Y.; Johnson, A. T. *Appl. Phys. Lett.* **2001**, *79*, 3326.
(23) Leonard, F.; Tersoff, J. *Phys. Rev. Lett.* **1999**, *83*, 5174.
(24) Louie, S. G. In *Carbon Nanotubes: Synthesis, Structure, Properties, and Applications*; Dresselhaus, M. S., Dresselhaus, G., Avouris, Ph., Eds.; Springer-Verlag: Berlin, Heidelberg, 2001.
(25) Rochefort, A.; Avouris, Ph. *Nano Lett.* **2002**, *2*, 253.
(26) Jiang, C.; Zhao, J.; Therese, H. A.; Friedrich, M.; Mews, A. *J. Phys. Chem. B* **2003**, *107*, 8742.
(27) Ditchburn, R. W. *Light*; Dover Publications: New York, 1961.

NL050053K